Catalysis Today 175 (2011) 460–466

Contents lists available at ScienceDirect

Catalysis Today

journal homepage: www.elsevier.com/locate/cattod

# Preparation of unsupported Ni–Mo–S catalysts for hydrodesulfurization of dibenzothiophene by thermal decomposition of tetramethylammonium thiomolybdates

Yanjiao Yi, Xin Jin, Lei Wang, Qiumin Zhang, Guang Xiong, Changhai Liang*

*Laboratory of Advanced Materials and Catalytic Engineering, School of Chemical Engineering, Dalian University of Technology, Dalian 116012, China*

ARTICLE INFO

*Article history:*
Received 14 October 2010
Received in revised form 24 February 2011
Accepted 23 April 2011
Available online 31 May 2011

*Keywords:*
Unsupported
Hydrodesulfurization
Thiomolybdates
Ni–Mo sulfides

ABSTRACT

Unsupported Ni–Mo sulfide catalysts were prepared by thermal decomposition of tetramethylammonium thiomolybdostate and nickel nitrate, which were characterized by Fourier transform infrared spectroscopy, ultraviolet–visible spectroscopy, thermogravimetric and differential thermal analysis, X-ray diffraction, $N_2$ physorption, elemental mapping and transmission electron microscopy. Hydrodesulfurization of dibenzothiophene was also performed in a fixed-bed reactor over the unsupported Ni–Mo sulfide catalysts. The results showed that the structures and properties of unsupported Ni–Mo sulfides depended on nickel content and decomposition conditions. Ni–Mo sulfides with type IV isotherms related to mesoporous structure were obtained. The layer and stacking degree of sulfide particles showed a decreasing trend, which leaded to a decrease of specific surface area, with increasing nickel content. All elements were homogeneously distributed, suggesting the "Ni–Mo–S" phase was formed. The addition of nickel promoted the dibenzothiophene conversion and the direct desulfurization pathway in the hydrodesulfurization of dibenzothiophene. The sample $Ni_{0.1}$–$MoS_2$ gave superior hydrodesulfurization activity for dibenzothiophene to other samples. The unsupported Ni–Mo sulfide catalysts exhibited desired activity in hydrodesulfurization and therefore might find wide applications in hydrotreating of fuel oil.



## 1. Introduction

More and more stringent environmental regulations and fuel specifications are demanding a significant reduction of sulfur and nitrogen containing compounds, as well as aromatics in fuels. Hydrodesulfurization (HDS) catalysts are of great importance on producing higher quality oil with lower sulfur content since the catalyst is "heart" of almost all refining processes. Conventional sulfide HDS catalysts are usually supported on $\gamma$-$Al_2O_3$ which can provide high dispersion of the active metal phase [1] and good mechanical properties. However, for their conventional preparation via oxide route, incomplete sulfidation caused by strong interaction between metal and support leads catalysts to the decrease in HDS activity. Unsupported catalysts without support can effectively settle the problem.

Recently, unsupported sulfide catalysts have attracted much attention due to their high activity in the hydrotreating reactions. A number of methods, including comaceration [2], homogeneous sulfide precipitation [3], thiosalt decomposition [4–6], hydrothermal and solvothermal processes [7–10] and solution reactions [11,12], have been used to prepare unsupported sulfide catalysts. The structures and catalytic properties of these sulfides obtained by the above methods depended strongly on their preparation and treatment conditions [2,3,9].

Thiosalt decomposition provides a simple and reproducible method for obtaining the unsupported sulfide materials with controlled stoichiometry and specific surface area. Ammonium thiosalts are typical precursors for synthesizing sulfides due to their sulfur bound to the metal atoms, which have been extensively studied by Bernard and Tridot [13] and Müller and Diemann [14], and improved in the synthesis techniques by McDonald et al. [15] and Pan et al. [16]. However, the sulfide catalysts reported in the following Ref. [3] are low in surface area and activity and more $NiS_x$ and $MoO_y$ impurities. A similar approach was developed by other groups leading to high activity and high surface area catalysts [17]. However, this preparation method is still in an early stage of development. A multi-metal compounds need to be tested and studied in detail because the resulted sulfides are potential catalysts in hydrotreating reactions. In this work, the unsupported nickel-promoted $MoS_2$ sulfides were prepared by ex situ decomposition of tetramethylammonium thiomolybdates and $Ni(NO_3)_2$.

* Corresponding author. Fax: +86 411 39893991.
*E-mail address:* changhai@dlut.edu.cn (C. Liang).
*URL:* http://finechem.dlut.edu.cn/liangchanghai (C. Liang).

0920-5861/$ – see front matter © 2011 Elsevier B.V. All rights reserved.
doi:10.1016/j.cattod.2011.04.039

The results show that the structures and catalytic properties of the unsupported Ni–Mo sulfides depended on nickel content and decomposition conditions.

## 2. Experimental

### 2.1. Preparation

Typically, 2.0 g hexaammonium heptamolybdate tetrahydrate $(NH_4)_6Mo_7O_{24}$ was dissolved in 7.0 ml aqueous ammonia. Then, 17.4 g ammonium sulfide was added in the solution at 338 K under stirring condition. After about 1.5 h, the deep red solution of ammonium thiomolybdate (ATM) was generated. After adding the water solution of tetramethylammomium chloride and sodium hydroxide, the red tetramethylammomium thiomolybdate (TMetATM) crystal was formed. Finally, TMetATM was obtained after being filtered and dried in the air.

In order to prepare the Ni–Mo sulfides with Ni/Ni + Mo molar ratios of 0, 0.1, 0.3, 0.5, the precursors of TMetATM and appropriate amount of nickel nitrate were mixed by mechanical grinding method. These precursors were heated to the final temperature in argon at a 3 °C/min rate of and cooled down to room temperature at flowing argon. The prepared samples were labeled as $MoS_2$, $Ni_{0.1}$–$MoS_2$, $Ni_{0.3}$–$MoS_2$ and $Ni_{0.5}$–$MoS_2$, respectively.

### 2.2. Characterization

Fourier transform infrared (FT-IR) spectra was collected at room temperature on a Fourier transform infrared spectrometer of model Nicolet Impact 410 with a resolution of 4 $cm^{-1}$, and ultraviolet–visible (UV–vis) spectra were recorded on a ultraviolet–visible spectrometer (JASCO V-550). Thermogravimetry (TG) and differential thermal analysis (DTA) were performed in Mettler Toledo TGA/SDTA851$^e$ thermogravimetry under nitrogen from room temperature to 450 °C at a heating rate of 10 °C/min to determinate their decomposition behavior. Specific surface area (SSA) measurements were performed on Micromertics 2010 instrument by nitrogen adsorption at −196 °C using the BET isotherm while the pore size distribution was calculated by $N_2$ adsorption using the Barrett–Joyner–Hallenda (BJH) method. The mean standard deviation for specific surface area measurements was about 2%. X-ray diffraction (XRD) analysis of the samples was carried out using a Rigaku D/Max-RB diffractometer with Cu Kα monochromatized radiation source (λ = 1.54178 A), operated at 40 kV and 100 mA. Particle size and distribution of the samples were studied by transmission electron microscopy (TEM) a Philips CM200 FEG transmission electron microscope (accelerating voltage 200 kV) using high-resolution imaging. Elemental mapping was conducted under STEM mode with the EDX detector as recorder.

### 2.3. Hydrodesulfurization of dibenzothiophene

Hydrodesulfurization of dibenzothiophene (DBT) was carried out in continuous mode in a fixed-bed reactor as described elsewhere [2]. A 0.05 g sample of passivated $MoS_2/Ni_x$–$MoS_2$ catalysts was diluted with quartz to achieve isothermal plug-flow conditions. The catalyst was activated in situ in $H_2$ (60 ml/min) at 613 K for 0.5 h to remove the passivation layer. After activation, the pressure was increased to 3.0 MPa and the temperature was kept at 613 K for the HDS reaction. The liquid reactant was fed into the reactor by means of a high-pressure pump. The composition of the liquid feed was 94.7 wt.% decalin as solvent, 0.3 wt.% n-octane (GC reference for DBT and its derivatives), and 5 wt.% DBT. The reaction products were analyzed on a gas chromatograph (GC 7890F) with flame ionization (FID) detector and a SE-54/52 capillary column.

## 3. Results and discussion

### 3.1. Precursors characterization

The reaction involves an acid–base process between the amine group and the ammonium ions in $(NH_4)_2MoS_4$ to produce ammonia and the corresponding $[(CH_3)_4N]_4MoS_4$. For the $(NH_4)_2MoS_4$ formation, the process occurs according to reaction (1):

$$(NH_4)_6Mo_7O_{24} + 28(NH_4)_2S \rightarrow 7(NH_4)_2MoS_4 + 48NH_3 + 24H_2O \quad (1)$$

Sodium hydroxide can improve the reaction rate since it decreases the concentration of the resultant $NH_4Cl$. For $[N(CH_3)_4]_2MoS_4$, we propose that the process occurs according to reactions (2) and (3):

$$(NH_4)_2MoS_4 + (CH_3)_4NCl \rightarrow [N(CH_3)_4]_2MoS_4 + NH_4Cl \quad (2)$$

$$NH_4Cl + NaOH \rightarrow NaCl + NH_3\uparrow + H_2O \quad (3)$$

The FT-IR spectrum for $[(CH_3)_4N]_2MoS_4$ was shown in Fig. 1 by using $(NH_4)_2MoS_4$ as a reference. The spectra of $[(CH_3)_4N]_2MoS_4$ and $(NH_4)_2MoS_4$ gave the bands corresponding to Mo–S stretching mode at 480 and 476 $cm^{-1}$ [18], respectively. Mo–S stretching bands shifted to lower wavenumber and their bond strength became weak after methyl group was added. This can be attributed to that the ability of methyl group donating electron was stronger than that of H atom. So that the positive charge density of methyl-substituted ammonium cation was lower than that of ammonium cation, thus the negative charge density of $MoS_4^{2*}$ decreased in tetramethylammonium thiomolybdates, which resulted to weakening the Mo–S bonds. These results were in agreement with previous results by Pan et al. [16] for molybdenum sulfide complexes and Müller et al. [14,19] for tetrathiometallate compounds. From the spectrum of $[(CH_3)_4N]_2MoS_4$, the wavenumber of 1384 $cm^{-1}$ indicates that methyl groups have successfully replaced H atoms.

UV–vis spectra of $[(CH_3)_4N]_2MoS_4$ and $(NH_4)_2MoS_4$ are shown in Fig. 2. Five main bands corresponding to thiomolybdate groups $MoS_4^{2-}$ were detected. For $[(CH_3)_4N]_2MoS_4$, the wavelength maximum appeared at 213, 234, 305, 446 and 549 nm while $(NH_4)_2MoS_4$ appeared at 211, 247, 310, 452 and 546 nm. The Mo complexes exhibited absorption bands in both visible and UV spectral regions. This is in agreed with previous study in our group [20].

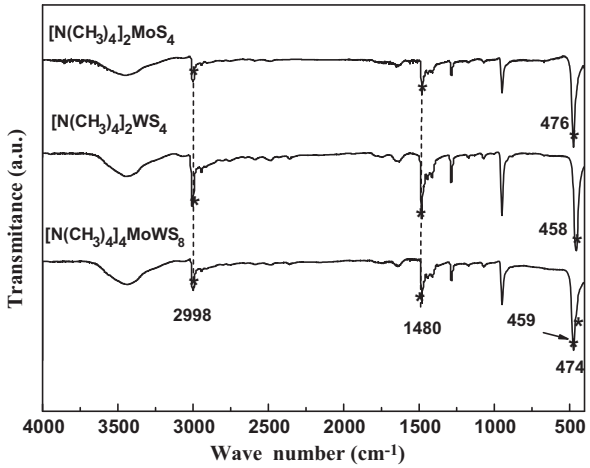


**Fig. 1.** FT-IR spectra of $[(CH_3)_4N]_2MoS_4$ and $(NH_4)_2MoS_4$.

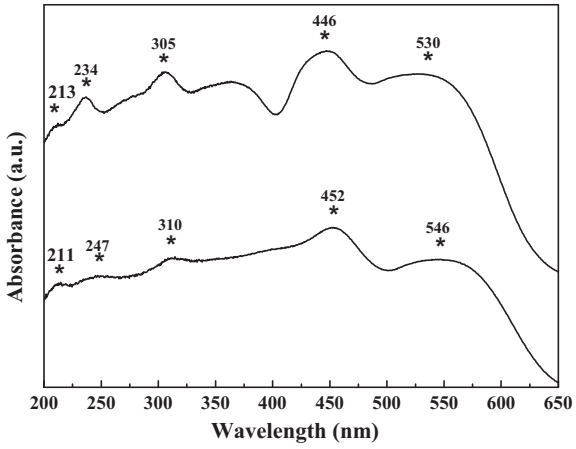


**Fig. 2.** UV–vis spectra of $[(CH_3)_4N]_2MoS_4$.

### 3.2. TG–DTA of $N(CH_3)_4]_2MoS_4$ and its mixture with $Ni(NO_3)_2{\cdot}6H_2O$

The decomposition of $[N(CH_3)_4]_2MoS_4$ and $Ni_3Mo_7S_{28}\{14[(CH_3)_4N]{\cdot}6NO_3\}{\cdot}3xH_2O$ was studied by TG–DTA (shown in Fig. 3). One step mass loss and one endothermic peak at 260.8 °C were found from the TG–DTA curves of $[N(CH_3)_4]_2MoS_4$, While two-step mass loss and one exothermic peaks appeared at 223.9 °C was found from those of $Ni_3Mo_7S_{28}\{14[(CH_3)_4N]{\cdot}6NO_3\}{\cdot}3xH_2O$. The related data were summarized in Table 1. For $[N(CH_3)_4]_2MoS_4$, the transitions as well as the weight losses were consistent with the reaction:

$$[N(CH_3)_4]_2MoS_4 \rightarrow (CH_3)_2S_2 + 2(CH_3)_3N + MoS_2 \quad (4)$$

The single step reaction (241–400 °C) was proposed to involve elimination of two molecules of methylamine $(CH_3)_3N$ and one molecule of methyl disulfide $(CH_3)_2S_2$. In this case, the methyl groups would react with the $S^{2-}$ ions of the $MoS_4^{2-}$ unit to give disulfide compounds. This result is similar to those previously reported [20–23].

For $Ni_3Mo_7S_{28}\{14[(CH_3)_4N]{\cdot}6NO_3\}{\cdot}3xH_2O$, a slight weight loss (8.4%) was observed at low temperature, maybe due to elimination of water and impurities. The decomposition mechanism of the bimetallic precursors was complicated due to the fact that nickel nitrate reacted first with the tetramethylammonium group to form bimetallic complexes [24], as shown in reaction (5):

$$7[(CH_3)_4N]_2MoS_4 + 3Ni(NO_3)_2{\cdot}xH_2O \rightarrow Ni_3Mo_7S_{28}\{14[(CH_3)_4N]{\cdot}6NO_3\}{\cdot}3xH_2O \quad (5)$$

The thermal decomposition of the $Ni_3Mo_7S_{28}\{14[(CH_3)_4N]{\cdot}6NO_3\}{\cdot}3xH_2O$

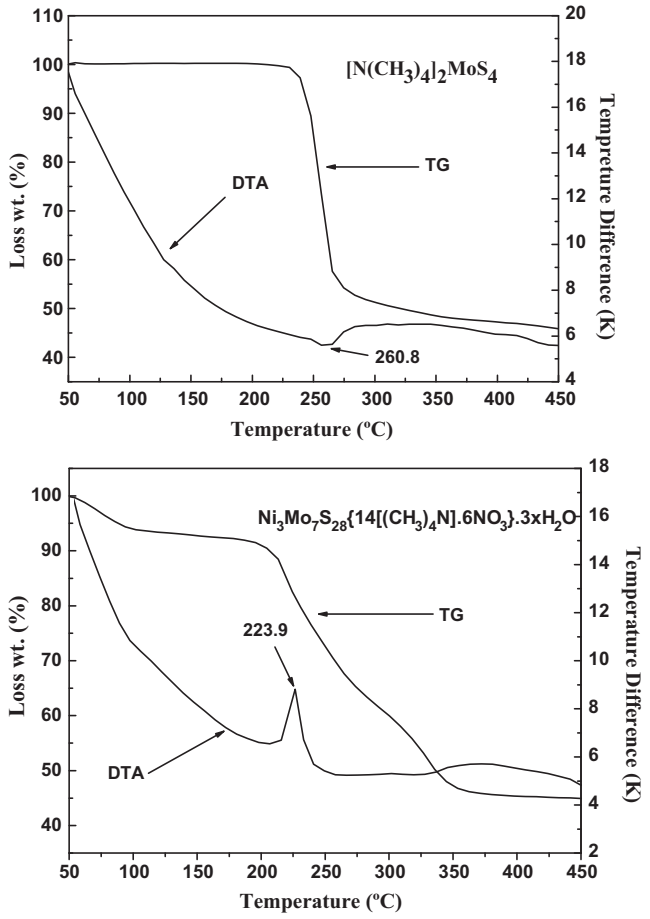


**Fig. 3.** TG–DTA curves of $[N(CH_3)_4]_2MoS_4$ and $Ni_3Mo_7S_{28}\{14[(CH_3)_4N]{\cdot}6NO_3\}{\cdot}3xH_2O$.

occurred in two steps and the reactions (6) and (7) were represented as follows:

$$Ni_3Mo_7S_{28}\{14[(CH_3)_4N]{\cdot}6NO_3\}{\cdot}3xH_2O \rightarrow 7Ni_{0.3}/MoS_3 + 14(CH_3)_3N + CH_3S + (CH_3)_2S + 6CH_3NO_3 \quad (6)$$

$$Ni_{0.3}/MoS_3 \rightarrow Ni_{0.3}/MoS_{3-x} + xS^0 \quad (7)$$

The decomposition of $Ni_3Mo_7S_{28}\{14[(CH_3)_4N]{\cdot}6NO_3\}{\cdot}3xH_2O$ was strongly exothermic and occurred between 175 and 400 °C with a weight loss of 47.1%. In this step, fourteen molecules of $(CH_3)_3N$, six molecules of $CH_3S$, one molecules of $(CH_3)_2S$ and six molecules of $CH_3NO_3$ were proposed to eliminate. This differs

**Table 1**
TG–DTA results for $[N(CH_3)_4]_2MoS_4$ and $Ni_3Mo_7S_{28}\{14[(CH_3)_4N]{\cdot}6NO_3\}{\cdot}3xH_2O$.

| Determinant | $[N(CH_3)_4]_2MoS_4$ | $Ni_3Mo_7S_{28}\{14[(CH_3)_4N]{\cdot}6NO_3\}{\cdot}3xH_2O$ |
|---|---|---|
| $T_1$ (°C) | 214 | 50 |
| $T_2$ (°C) | 400 | 175 |
| $w_1$ (wt.%) ($exp_{1-2}$) loss | 55 | 8.4 |
| $w_2$ (wt.%) ($theor_{1-2}$) loss | 57 | – |
| Assuming loss of | $(CH_3)_2S_2 + 2(CH_3)_3N$ | $H_2O$ |
| $T_3$ (°C) | – | 400 |
| $w_2$ (wt.%) ($exp_{3-4}$) loss | – | 47.1 |
| Assuming loss of | – | $14(CH_3)_3N + 6CH_3S + (CH_3)_2S + 6CH_3NO_3 + xS^0$ |
| Residual (wt.%) (exp) | 45 | 44.5 |
| Residual (wt.%) (theor) | 43 | – |
| Assuming final product | $MoS_2$ | $Ni_{0.3}$–$MoS_{3-x}$ |

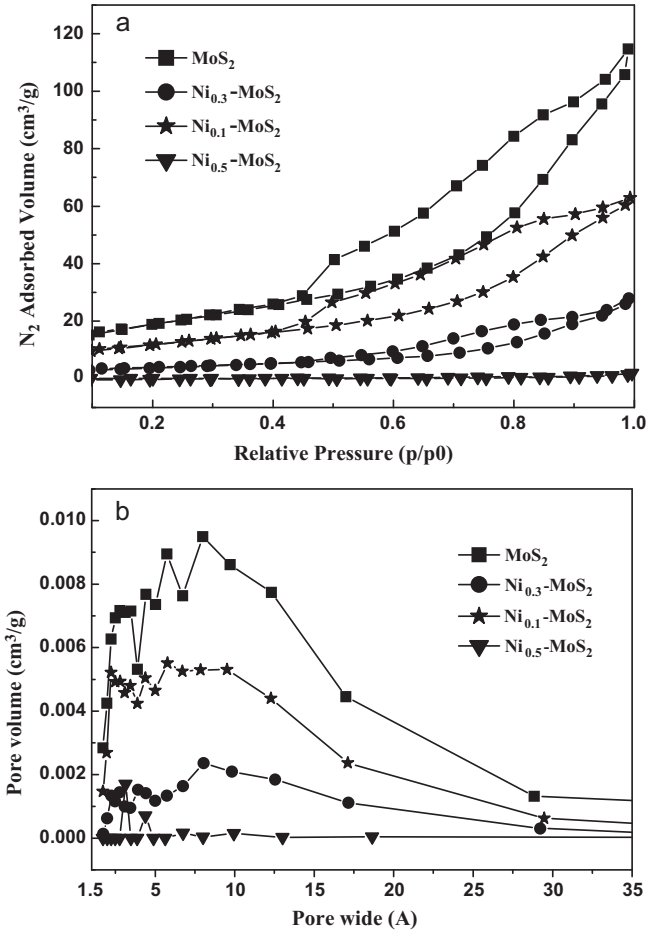


**Fig. 4.** Adsorption–desorption isotherms for unsupported $MoS_2$ and Ni–Mo sulfides (a) and pore size distribution calculated by BJH method for unsupported $MoS_2$ and Ni–Mo sulfides (b).

completely from the decomposition behaviors observed from the precursors without nickel.

### 3.3. Characterization

The ex situ decomposition of tetramethylammonium thiomolybdate and its mixture with nickel nitrate was used to generate $MoS_2$ and $Ni_x$–$MoS_2$. This method leads to moderate SSA and type IV and I adsorption–desorption nitrogen isotherms, poorly crystalline structures, homogeneous "Ni–Mo–S" phase generation and desired activity in the HDS of DBT.

#### 3.3.1. Nitrogen physorption

Fig. 4a presents the $N_2$ adsorption–desorption isotherms of Ni–Mo sulfides. As observed in Fig. 4a, $MoS_2$, $Ni_{0.1}$–$MoS_2$ and $Ni_{0.3}$–$MoS_2$ present similar type IV adsorption–desorption isotherms with a desorption step characteristic of mesoporous materials. The nickel content in the thiosalt precursor strongly influences the porous texture of the final sulfides. For $Ni_{0.5}$–$MoS_2$ sample, a poor developed porous system was observed with average diameter close to 6.05 nm and type I adsorption isotherm. The $MoS_2$ sample exhibited a most well-defined hysteresis loop characteristic of a well developed porous texture comparing with other sulfides. Broad range of pore volume (from 0.010 to 0.178 $cm^3/g$) of the obtained sulfides was considered from decomposition of methyl fragments, which escaped from the precursor during the process. The reaction enthalpy has an important influence on the formation of cavities upon the decomposition of organic fragments.

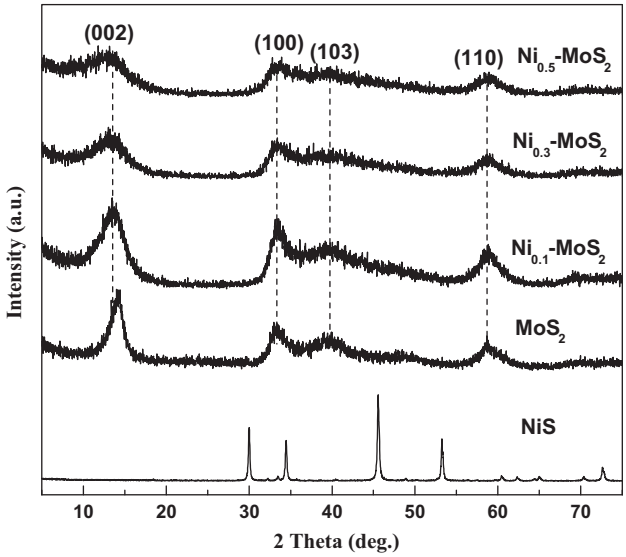


**Fig. 5.** XRD patterns of NiS, $MoS_2$ and $Ni_x$–$MoS_2$ ($x$ = 0.1, 0.3, 0.5).

Cavities are formed by the accumulation of gases while channels are created during the escape of these gases.

Fig. 4b shows the BJH pore-size distributions of the prepared sulfides. As seen from Fig. 4b, a broad pore size distribution from 2 to 17 nm were found for $MoS_2$, $Ni_{0.1}$–$MoS_2$ and $Ni_{0.3}$–$MoS_2$ while $Ni_{0.5}$–$MoS_2$ a narrow pore size distribution curves centered at 3 nm in diameter was obtained. The SSA, mean pore size and pore volume of the as-prepared sulfides are shown in Table 2. Nickel content in the tetramethylammonium precursors has an important effect on SSA and pore volume of the sulfides. Compared with $Ni_{0.1}$–$MoS_2$, $Ni_{0.3}$–$MoS_2$ and $Ni_{0.5}$–$MoS_2$ prepared from tetramethylammonium precursors, the non-promoted $MoS_2$ has the highest specific surface area of 68 $m^2/g$. Interestingly, the SSA continuously decreases from 44 to 9 $m^2/g$ with increasing nickel content in prepared sulfides.

#### 3.3.2. X-ray diffraction

The XRD patterns of the as-prepared sulfides (see Fig. 5) show characteristic crystalline structure of $MoS_2$, with the significant reflections $2\theta$ at 14.1° (0 0 2), 33° (1 0 0), 39° (1 0 3) and 59° (1 1 0). The intensity of the (0 0 2) peak is representative for the stacking of the slabs along the $c$-axis while the intensity of the (1 1 0) peak is representative for the layer of the slabs. As shown in Fig. 5, when nickel concentration increases from 0.1 to 0.5, the intensity of the (0 0 2) signal gradually decreases, which demonstrates a marked stacking diminution of the sulfide particle slabs. No obviously peaks of nickel, nickel oxide and nickel sulfide were observed especially NiS (Fig. 5), indicating that nickel was highly dispersed on $MoS_2$ or with rather small particles. $MoO_x$ were still not found from the XRD patterns of the sulfides prepared after the mechanical grinding and decomposition steps.

#### 3.3.3. Transmission electron microscopy and elemental mapping

Fig. 6 presents the transmission electron microscopy (TEM) micrographs of $MoS_2$ and $Ni_x$–$MoS_2$ samples. The sulfides revealed the presence of typical structures of the layer like $MoS_2$ phase. The $MoS_2$ sample has greater stacking in the (0 0 2) direction and longer layers than the other samples. Qualitative analysis revealed that $MoS_2$ consisted in three to seven stacked layers and the slab length of fringes reaches values up to 8 nm. The stacking degree of $Ni_{0.1}$–$MoS_2$ sample is estimated to be 2–6 slabs and the slabs length was about 5 nm while $Ni_{0.3}$–$MoS_2$ has a stacking of 2–5 layers of average length about 4 nm. For $Ni_{0.5}$–$MoS_2$ (Fig. 6d) sample entangled $Ni_{0.5}$–$MoS_2$ slabs were rather difficult to analyze

**Table 2**
Specific surface area, pore volume, mean pore size, DBT conversion, product selectivity and HYD/DDS radio for unsupported bimetallic Ni–Mo sulfide catalysts.

| Catalyst | Specific surface area ($m^2/g$) | Pore volume ($cm^3/g$) | Mean pore size (nm) | DBT conversion (%) | Selectivity (%) | | | HYD/DDS |
|---|---|---|---|---|---|---|---|---|
| | | | | | BP | THDBT | CHB | |
| $MoS_2$ | 68 | 0.1775 | 10.37 | 15 | 59.2 | 17.5 | 23.3 | 0.5 |
| $Ni_{0.1}$–$MoS_2$ | 44 | 0.043 | 11.88 | 40 | 78.7 | 4.1 | 17.2 | 0.2 |
| $Ni_{0.3}$–$MoS_2$ | 23 | 0.097 | 8.95 | 29 | 85.0 | 3.2 | 11.8 | 0.2 |
| $Ni_{0.5}$–$MoS_2$ | 9 | 0.010 | 6.05 | 16 | 87.2 | 3.0 | 9.8 | 0.1 |

statistically since the particles overlapped. It is clear that the $Ni_{0.5}$–$MoS_2$ layers are quite distorted and twisted corresponding to the poorly crystalline or 'rag' in $MoS_2$ structure [25]. After nickel nitrate was added, the $MoS_2$ slabs give a more divided and collapsed trend, which has agreement with XRD results. Within the $MoS_2$ layers nickel was homogeneously distributed, suggesting the formation of "Ni–Mo–S" phase.

From elemental mapping of $Ni_{0.3}$–$MoS_2$ sample (Fig. 7), it can be clearly seen that nickel, sulfur and molybdenum elements have homogeneously distributed in the analyzed superficial zone. This further proves the formation of the "Ni–Mo–S" phase.

### 3.4. HDS of DBT

HDS mechanism of DBT over metal sulfide catalysts has shown that DBT undergo HDS by two reaction pathways: direct desulfurization (DDS) and hydrogenation (HYD). Scheme 1 shows these pathways for the HDS of DBT. In the DDS pathway, biphenyl (BP) is formed by hydrogenolysis or elimination reactions [26–28]. In the HYD pathway, the hydrogenated intermediates first are yielded, and the sulfur is then removed to form cyclohexylbenzene (CHB) and bicyclohexyl. The conversions of DBT and the product selectivities in Table 2 were obtained at 340 °C and 3.0 MPa. All of the samples produced three reaction products: BP, CHB, and tetrahydro-dibenzothiophene (THDBT).

The result reveals that the addition of nickel has an evident impact on BP products selectivity and DBT conversion. After adding nickel in the catalyst, total DBT conversion has an obvious increase from 15% to 40% by comparing $MoS_2$ and $Ni_{0.1}$–$MoS_2$ even though the surface area decreased. DBT conversion for $Ni_{0.3}$–$MoS_2$ and $Ni_{0.5}$–$MoS_2$ have a gradually decrease compared with $Ni_{0.1}$–$MoS_2$. This may due to the SSA decreasing and less active sites. Nickel in sulfide catalyst improving DBT conversion due to it exhibits an ability to promote Mo(W)–S interactions that can be attributed to electronic effects induced by metal–metal interactions. This improving effect can be better for catalysts presenting large areas, due to a larger number of the active sites [29].

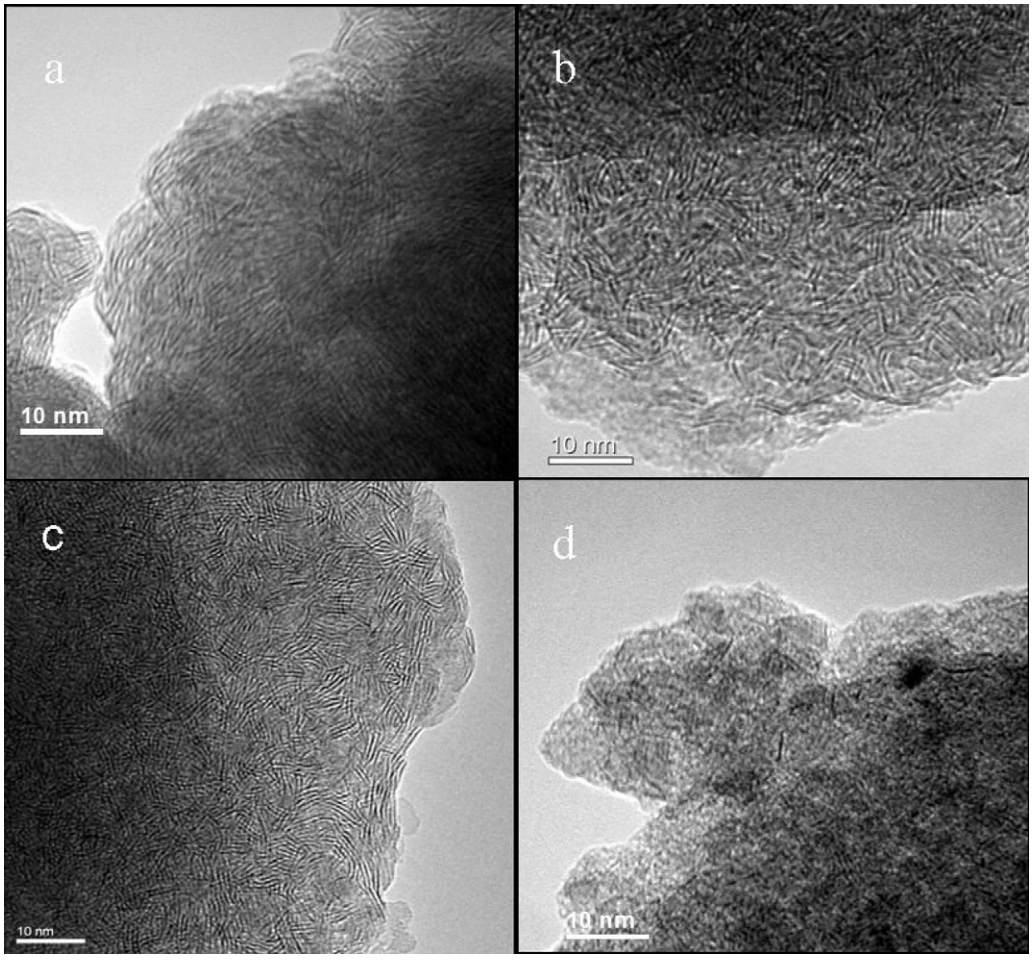


**Fig. 6.** Transmission electron micrograph of the $MoS_2$ and $Ni_x$–$MoS_2$: (a) $MoS_2$, (b) $Ni_{0.1}$–$MoS_2$, (c) $Ni_{0.3}$–$MoS_2$, and (d) $Ni_{0.5}$–$MoS_2$.

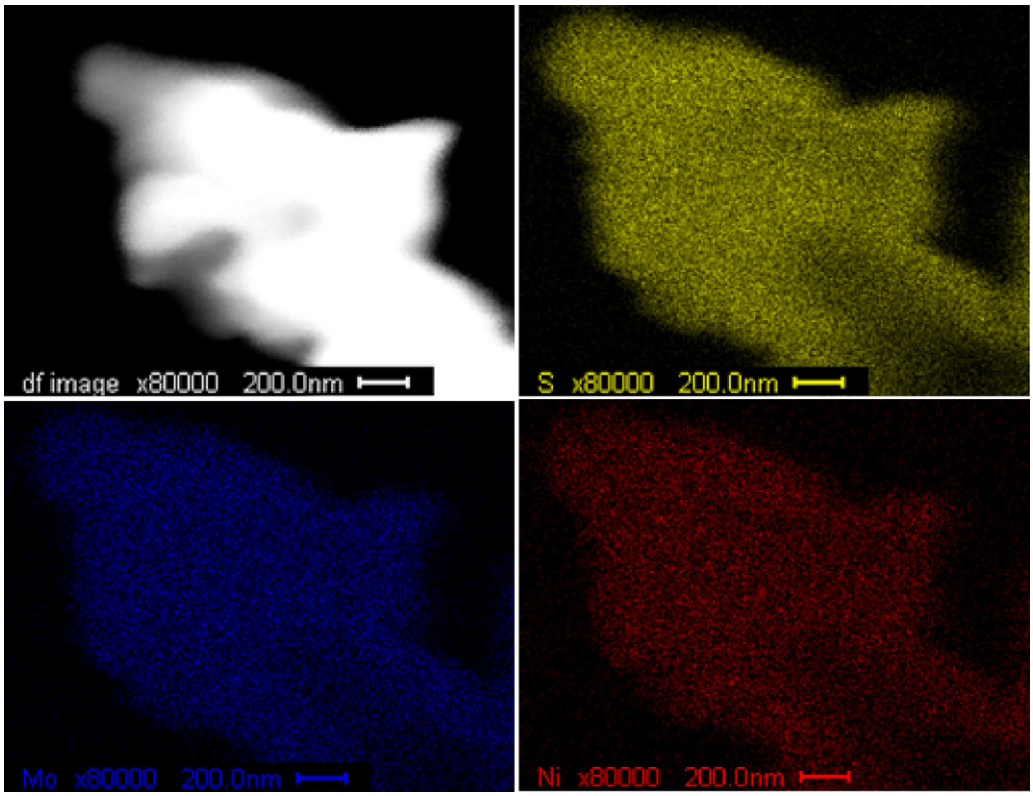


**Fig. 7.** Elemental mapping of the $Ni_{0.3}$–$MoS_2$ catalyst before HDS reaction by transmission electron microscopy.

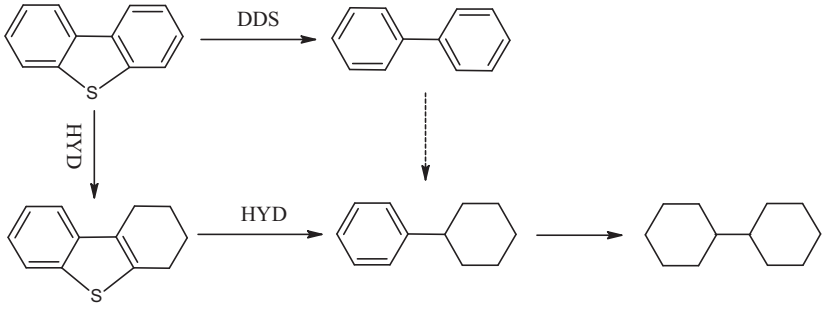


**Scheme 1.** HDS reaction pathways of DBT.

With the increasing nickel content in sulfide catalysts, BP selectivity gradually increased from 59.2% to 87.2% while CHB electivity reduced from 23.3% to 9.8% as well as THDBT from 17.2% to 3.0%. HYD/DDS ratio can be approximated using equation {[CHB] + [THDBT]}/[BP]. It has a significant decreasing from 0.5 to 0.1 with nickel concentration increasing from $MoS_2$ to $Ni_{0.5}$–$MoS_2$ catalyst. Selectivity for the HDS of DBT was shifted to the DDS route due to confining effects inside the mesoporous structure [6]. In the rim–edge model developed by Daage and Chianelli [30], two types of sites are located on stacked $MoS_2$ layers: the "rim" sites on top and bottom layers able both to hydrogenate and cleave C–S bonds and "edge" sites located on internal layers and only able to cleave C–S bonds. The differentiation between these two kinds of sites was related to steric hindrance on "edge" sites hampering the $g^6$ adsorption of the DBT molecule, prerequisite for the hydrogenation step. In fact, as already observed for $MoS_2$ catalysts [5,6,31], the high DDS selectivity would be a direct consequence of the mesoporous character of these catalysts leading to confinement effects restricting the sterically demanding $g^6$ adsorption on "rim" sites of $MoS_2$ layers located inside mesoporous cavities. This confinement effects become apparently when the pore side and volume decrease. An interesting feature to underline was related to the selectivity results for the $Ni_{0.5}$–$MoS_2$ in situ catalyst. The HYD/DDS ratio was quite low (0.1) showing an enhanced DDS selective character. Since the promotion by Ni is known to increase the C–S bond cleavagerate [27], this higher DDS selective character suggests that the nickel atoms were still involved in a promoted Ni–Mo phase.

## 4. Conclusions

Ni–Mo sulfide catalysts had been prepared by thermal decomposition of tetramethylammonium biometallates obtained by mechanical grinding of dimethylammonium thiomolybdate and nickel nitrate. The obtained sulfides showed type IV isotherms related to mesoporous structure, except $Ni_{0.5}$–$MoS_2$. The addition of nickel in sulfides leads to a decrease of specific surface area. With increasing nickel content, the layer and stacking degree of sulfide particles showed a decreasing trend. Nickel sulfide was not found in the samples by TEM study and elemental mapping showed that all elements (Ni–Mo) are homogeneously distributed, suggesting

the formation of "Ni–Mo–S" phase. The addition of nickel in sulfides promotes DBT conversion and direct desulfurization pathway in the HDS of DBT. The sample $Ni_{0.1}$–$MoS_2$ gave superior HDS properties for DBT to other samples.

## Acknowledgements

We gratefully acknowledge the financial support provided by the Program for New Century Excellent Talents in Universities of China (NCET-07-0133) and by the Research Fund for the Doctoral Program of Higher Education (20070141048).

## References

[1] H. Topsøe, B.S. Clausen, Appl. Catal. 25 (1986) 273.
[2] H. Ishihara, T. Itoh, T. Hino, M. Nomura, P. Qi, T. Kabe, J. Catal. 140 (1993) 184.
[3] K.S. Liang, R.R. Chianelli, F.Z. Chien, S.C. Moss, J. Non-Cryst. Solids 79 (1986) 251.
[4] D. Genuit, P. Afanasiev, M. Vrinat, J. Catal. 235 (2005) 302.
[5] H. Nava, C. Ornelas, A. Aguilar, G. Berhault, S. Fuentes, G. Alonso, Catal. Lett. 86 (2003) 257.
[6] G. Alonso, G. Berhault, A. Aguilar, V. Collins, C. Ornelas, S. Fuentes, R.R. Chianelli, J. Catal. 208 (2002) 359.
[7] Y.Y. Peng, Z.Y. Meng, C. Zhong, J. Lu, W.C. Yu, Z.P. Yang, Y.T. Qian, J. Solid State Chem. 159 (2001) 170.
[8] W.J. Li, E.W. Shi, J.M. Ko, Z.Z. Chen, H. Ogino, T. Fukuda, J. Cryst. Growth 250 (2003) 418.
[9] E. Devers, P. Afanasiev, B. Jouguet, M. Vrinat, Catal. Lett. 82 (2002) 13.
[10] N. Rueda, R. Bacaud, M. Vrinat, J. Catal. 169 (1997) 404.
[11] P. Afanasiev, G.F. Xia, G. Berhault, B. Jouguet, M. Lacroix, Chem. Mater. 11 (1999) 3216.
[12] I. Bezverkhy, P. Afanasiev, M. Lacroix, Inorg. Chem. 39 (2000) 5416.
[13] J.C. Bernard, G. Tridot, Bull. Soc. Chim. Fr. 5 (1961) 810.
[14] A. Müller, E. Diemann, Chem. Phys. Lett. 9 (1971) 369.
[15] J.W. McDonald, G. Delbert Friesen, L.D. Rosenhein, W.E. Newton, Inorg. Chim. Acta 72 (1983) 205.
[16] W.H. Pan, M.E. Leonowicz, E.I. Stiefel, Inorg. Chem. 22 (1983) 672.
[17] N. Berntsen, T. Gutjahr, L. Loeffler, J.R. Gomm, R. Seshadri, W. Tremel, Chem. Mater. 15 (2003) 4498.
[18] G. Alonso, G. Berhaualt, R.R. Chianelli, Inorg. Chim. Acta 316 (2001) 105.
[19] A. Müller, W. Hellmann, J. Schneider, U. Schimanski, U. Demmer, A. Trautwein, U. Bender, Inorg. Chim. Acta 65 (1982) L41.
[20] X. Jin, C.L. Ma, Y.J. Yi, Q.M. Zhang, J.S. Qiu, C.H. Liang, J. Phys. Chem. Solids 71 (2010) 12571.
[21] G. Alonso, G. Aguirre, I.A. Rivero, S. Fuentes, Inorg. Chem. Acta 274 (1998) 108.
[22] G. Alonso, M. Del Valle, J. Cruz, V. Petranovskii, A. Licea-Claverie, S. Fuentes, Catal. Today 43 (1998) 117.
[23] J.L. Brito, M. Ilija, P. Hernandez, Thermochim. Acta 256 (1995) 325.
[24] F. Pedraza, S. Fuentes, Catal. Lett. 65 (2000) 107.
[25] R.R. Chianelli, E.B. Prestidge, T.A. Pecoraro, J.P. Deneufville, Science 203 (1979) 1105.
[26] T. Todorava, R. Prins, T. Weber, J. Catal. 236 (2005) 190.
[27] F. Bataille, J.L. Lemberton, P. Michaud, G. Perot, M. Vrinat, M. Lemaire, E. Schulz, M. Breysse, S. Kasztelan, J. Catal. 191 (2000) 409.
[28] G.H. Singhal, R.L. Espino, J.E. Sobel, J. Catal. 67 (1981) 446.
[29] A. Olivas, D.H. Galvan, G. Alonso, S. Fuentes, Appl. Catal. A Gen. 352 (2009) 10.
[30] M. Daage, R.R. Chianelli, J. Catal. 149 (1994) 414.
[31] L. Alvarez, J. Espino, C. Ornelas, J.L. Rico, M.T. Cortez, G. Berhault, G. Alonso, J. Mol. Catal. A Chem. 210 (2004) 105.